

Proceeding Paper

Experimental and Analytical Study of SHS Aluminium Members under Uniform Compression [†]

Vincenzo Piluso  and Alessandro Pisapia * 

Department of Civil Engineering, University of Salerno, 84084 Fisciano, Italy; v.piluso@unisa.it

* Correspondence: alpisapia@unisa.it

[†] Presented at the 15th International Aluminium Conference, Québec, QC, Canada, 11–13 October 2023.

Abstract: The aim of this work was to study the ultimate behaviour of box-shaped aluminium members subjected to uniform compression. Eight stub column tests have been carried out at the University of Salerno. In particular, four box sections made of 6060 aluminium alloys with different width-to-thickness ratios have been investigated. The results have been reported in terms of the maximum compressive resistance and corresponding deformation capacity. Subsequently, the experimental results have been compared with those obtained by two accurate methodologies: (1) a theoretical procedure based on the deformation theory of plasticity (J2); and (2) an extension of the effective thickness method (ETM) provided by Annex L of the Eurocode 9 draft. These approaches take into account the local buckling effects within the elastic-plastic region, the strain-hardening behaviour of the aluminium material, and the interaction between the plate elements constituting the cross-section. Finally, a comparison between new methodologies and current design rules has been presented.

Keywords: aluminium alloys; box-shaped member; stub test; Eurocode 9; uniform compression; local buckling

1. Introduction

The utilization of aluminium alloys is experiencing significant growth in the realm of structural engineering applications, particularly in the context of long-span roof systems, movable bridges, and prefabricated frameworks. Aluminium possesses highly enticing characteristics, including a remarkable strength-to-weight ratio, exceptional resistance against corrosion, flexibility in accommodating varied cross-section shapes, an advantageous life-cycle cost, and expedient fabrication processes [1–3].

Aluminium alloys also exhibit structural disadvantages: high initial cost, high deformability resulting from an elastic modulus one-third that of steel, increased local and global stability issues, high sensitivity to thermal variations, and reduced strength due to heat-treated zones in welded areas. Similar to all metallic elements, aluminium alloy elements are sensitive to instability phenomena. One of the main stability problems for metal alloys is local buckling, which impacts the ultimate behavior of compressed portions of the cross-section and subsequently influences the ultimate resistance and plastic deformation capacity. This factor becomes even more significant for aluminium alloys given their lower elastic modulus. Local buckling is influenced by the slenderness of the cross-section, with buckling occurring in either the elastic or plastic range, depending on the ratio of width to thickness of the plate elements composing the member section. The European code, EN 1999-1-1 [4], establishes a classification method for cross-sections that considers the slenderness of the individual plate elements and the conventional elastic limit, $f_{0.2}$.

The current approaches for metal members are based on an elastic-perfectly plastic analysis performed on an effective cross-section. However, this approach [5] neglects two main aspects: (1) the real behaviour of the material, which is relevant for aluminium



Citation: Piluso, V.; Pisapia, A. Experimental and Analytical Study of SHS Aluminium Members under Uniform Compression. *Eng. Proc.* **2023**, *43*, 39. <https://doi.org/10.3390/engproc2023043039>

Academic Editor: Mario Fafard

Published: 25 September 2023



Copyright: © 2023 by the authors. Licensee MDPI, Basel, Switzerland. This article is an open access article distributed under the terms and conditions of the Creative Commons Attribution (CC BY) license (<https://creativecommons.org/licenses/by/4.0/>).

members because of their continuous strain-hardening behaviour [3]; and (2) the interaction between the plate elements constituting the cross-sections.

Many research studies have been dedicated to enhancing the accuracy in forecasting the ultimate response of aluminium alloy members. Numerous stub column tests have been performed on different cross-sectional shapes in order to acquire additional insights into the impact of local buckling phenomena on the ultimate resistance. Faella et al. [6] examined sections of a square hollow section (SHS) and a rectangular hollow section (RHS), providing an empirical formulation for computing the strain that corresponds to the complete development of local buckling. Su et al. [7] undertook an exhaustive experimental campaign on SHS and RHS sections fabricated from aluminium alloys 6061-T6 and 6063-T5, both with and without internal stiffeners.

In the study of Moen et al. [8], they investigated the behavior of aluminium alloy beams subjected to both uniform and non-uniform bending. They performed three- and four-point bending tests on beams made of aluminium alloys 6082-T4, 6082-T6, and 7108-T7. They found that the rotation capacity of these beams is influenced by the strain-hardening characteristics of the aluminium material and the magnitude of the moment gradient. In a more recent study, Wang et al. [9] performed experiments on extruded I-shaped beams made of 6000 series aluminium alloy. These beams were tested both with and without intermediate stiffeners under concentrated loads. Furthermore, Piluso et al. [10], Montuori et al. [11,12], and Pisapia [13,14] have proposed mathematical equations to calculate the ultimate flexural strength and rotation capacity of box-shaped (SHS and RHS) and I-shaped aluminium beams.

Following the research provided by NASTRI et al. [15,16], a variation of the effective thickness method (ETM), which is currently utilized by Eurocode 9 [4], has been formulated to calculate the ultimate resistance of aluminium beams. This revised edition of ETM is currently presented in Annex L of the revised version of Eurocode 9 [17].

In recent years, there has been a significant advancement in the understanding of the inelastic response of aluminium compression members. However, there still exists a significant deficiency in experimental data compared to steel members. In order to address this issue, the University of Salerno conducted eight stub column tests on square hollow section (SHS) members. These members were made of 6060 aluminium alloys and varied in terms of their width-to-thickness ratios. Subsequently, the experimental results were obtained in terms of maximum compression resistance and maximum strains. Then, two accurate methodologies were presented: (1) a theoretical procedure based on the deformation theory of plasticity (J2) [18–20]; and (2) an extension of the effective thickness method (ETM) provided by Annex L of the Eurocode 9 draft [4]. These approaches consider the local buckling effects in the elastic-plastic range, the strain-hardening behaviour of aluminium material, and the interaction between the plate elements constituting the cross-section. Finally, the experimental results presented in this work with those provided in [6,7] have been compared with the theoretical results obtained by means of the previous methodologies and current design provisions.

2. Experimental Campaign

2.1. Geometric and Mechanical Properties

The aluminium members analysed in the current experimental tests are extruded beams made of EN-AW 6060 T66 with the SHS section.

Four types of section are considered for both stub and bending tests, characterized by a nominal width of 40, 60, 80, or 100 mm and with the same nominal thickness equal to 2 mm. According to Figure 1, the nominal and measured geometrical properties of specimens are reported in Table 1.

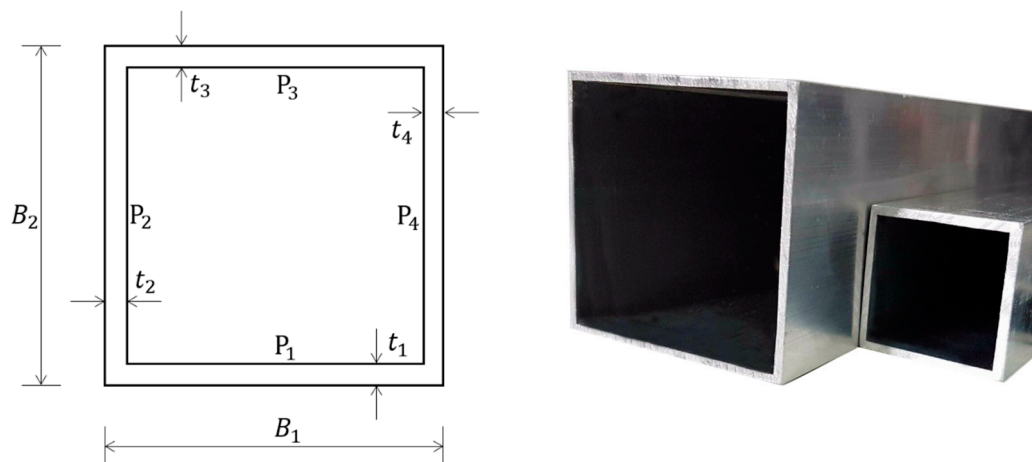


Figure 1. Geometric scheme of box section.

Table 1. Nominal and measured geometric properties of tested specimens.

Section	$B_{1,nom}$ [mm]	$B_{2,nom}$ [mm]	t_{nom} [mm]	A_{nom} [mm ²]	B_1 [mm]	B_2 [mm]	t_1 [mm]	t_2 [mm]	t_3 [mm]	t_4 [mm]	A [mm ²]
SHS40	40.00	40.00	2.00	304	40.18	40.11	1.99	2.20	2.09	2.00	315.26
SHS60	60.00	60.00	2.00	464	60.31	60.40	2.00	2.16	2.00	2.09	480.92
SHS80	80.00	80.00	2.00	624	80.17	80.06	2.00	1.98	1.90	1.89	607.40
SHS100	100.00	100.00	2.00	784	100.30	100.30	2.24	2.04	2.12	2.37	860.40

Standard tensile tests have been performed on specimens cut from each type of section according to UNI-EN-ISO 6892-1-1 [21]. In particular, the specimens P_1 were cut from each plate constituting the section according to the shape shown in Figure 2. The geometric dimensions are reported in Table 2.

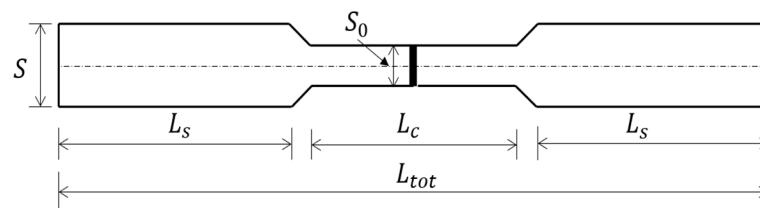


Figure 2. Geometric scheme of the material tensile coupon.

Table 2. Geometric properties of tensile coupons.

Section	S_0 [mm]	S [mm]	L_c [mm]	L_s [mm]	L_{tot} [mm]
SHS40	15	30	80	90	275
SHS60	15	30	80	90	275
SHS80	20	40	100	100	320
SHS100	20	40	100	100	320

The monotonic tests have been performed under displacement control according to Method A2 as described in UNI-EN-ISO 6892-1-1 [21]. The experimental results for each plate constituting each tested section are reported in Table 3. In particular, the following measured properties are provided:

- The experimental Young's modulus [E_{exp}]
- The stress at a residual strain of 0.1% [$f_{0.1}$]
- The stress at a residual strain of 0.2% [$f_{0.2}$]
- The engineering maximum stress [f_u]
- The engineering strain corresponding to the maximum stress [ε_u]
- The ultimate strain [ε_r]
- The Ramberg–Osgood coefficient [n] given by:

Table 3. Mechanical properties of tested tensile coupons.

Specimen		E_{exp} [mPa]	$f_{0.1}$ [mPa]	$f_{0.2}$ [mPa]	f_u [mPa]	ε_u [-]	ε_r [-]	n_i [-]	n_p [-]
SHS 40	P ₁	73054	171.00	181.75	207.85	0.055	0.075	11.34	22.96
	P ₂	75767	176.70	182.59	203.03	0.046	0.062	21.14	28.22
	P ₃	71465	160.83	174.03	202.17	0.053	0.074	8.78	20.35
	P ₄	66793	154.92	166.92	192.36	0.057	0.072	9.29	23.53
SHS 60	P ₁	65669	210.11	227.32	252.65	0.054	0.064	8.80	30.38
	P ₂	61254	207.09	215.00	238.83	0.065	0.088	18.49	33.09
	P ₃	65277	224.68	231.39	252.22	0.065	0.082	23.55	38.62
	P ₄	72674	213.20	226.59	253.58	0.069	0.095	11.38	31.90
SHS 80	P ₁	69665	210.82	224.17	246.02	0.039	0.064	11.29	35.70
	P ₂	75975	199.00	211.00	253.41	0.061	0.068	11.84	18.66
	P ₃	65174	226.46	236.92	255.41	0.042	0.050	15.35	39.65
	P ₄	63341	217.45	231.12	253.71	0.070	0.091	11.37	38.07
SHS 100	P ₁	71564	168.65	174.75	199.10	0.060	0.088	19.51	26.39
	P ₂	70044	165.38	175.61	201.80	0.060	0.098	11.55	24.83
	P ₃	66906	140.02	152.86	187.38	0.080	0.103	7.90	17.64
	P ₄	69317	155.32	169.36	195.79	0.060	0.085	8.00	22.51

$$n_i = \frac{\ln 2}{\ln\left(\frac{f_{0.2}}{f_{0.1}}\right)} \quad n_p = \frac{\ln(0.002/\varepsilon_{0,u})}{\ln\left(\frac{f_{0.2}}{f_u}\right)} \quad (1)$$

n_i and n_p are, respectively, the R-O coefficients in the inelastic and plastic region and $\varepsilon_{0,u}$ is the residual strain corresponding to the maximum stress f_u , it is equal to $\varepsilon_{0,u} = \varepsilon_u - 0.002$. The Ramberg–Osgood law is given by:

$$\varepsilon = \frac{\sigma}{E} + 0.002 \left(\frac{\sigma}{f_{0.2}} \right)^n \quad (2)$$

2.2. Stub Column Tests

Stub column tests have been carried out to evaluate the maximum load $N_{u,exp}$ and corresponding displacement $\delta_{u,exp}$ of SHS aluminium members. The test setup is shown in Figure 3. The compression tests were provided by means of a Schenck Hydropuls S56 testing machine (maximum load 630 kN, piston stroke ± 125 mm). For each member, a minimum of two stub tests were tested. The loading protocol is based on the application of two different test speeds, equal for each specimen: an initial low speed v_i equal to 0.42 mm/min up to post-elastic level and, successively, a final speed v_f equal to 1.20 mm/min. The speed change was set for each specimen according to the theoretical yield displacement $\delta_{0.2}$.

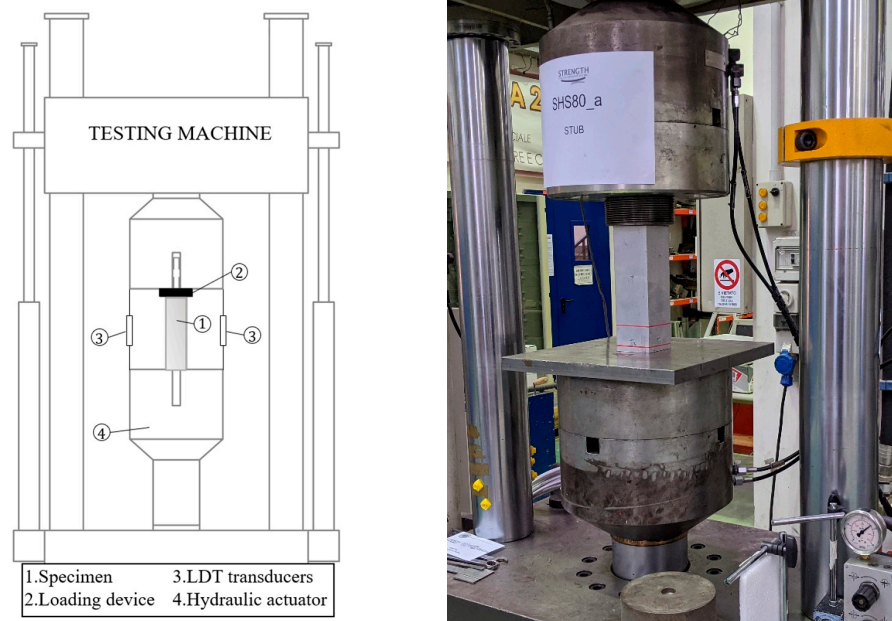


Figure 3. Geometric scheme of the material tensile coupon.

The axial displacements have been measured by three inductive transducers (LDT). The mean value of the three measures was considered. Almost all the specimens have failed due to pure local buckling, except the tests referring to SHS100 (test a, test b) and SHS80 (test a) where the instability phenomenon occurred, preliminarily, of a single plate due to the geometrical imperfections of sections and as can also be depicted by observing the shapes of $N - \delta$ curves provided in Figure 4. The results are shown in Table 4, where the specimen height a , the ultimate resistance $N_{u.exp}$ its non-dimensional value \bar{N}_u , the maximum displacement $\delta_{u.exp}$, and its non-dimensional value $\bar{\delta}_u$ are provided. The non-dimensional values are expressed as:

$$\bar{N}_u = \frac{N_{u.exp}}{A \cdot f_{0.2}} \quad \bar{\delta}_u = \frac{\delta_{u.exp}}{\delta_{0.2}} \tag{3}$$

where A represents the section area of each section, while $\delta_{0.2}$ corresponds to the displacement according to the conventional strain $\epsilon_0 = f_{0.2}/E$. Consequently, considering that $\delta = \epsilon \cdot a$, $\bar{\delta}_u$ coincides with the normalised buckling strain $\bar{\epsilon}_u$:

$$\bar{\epsilon}_u = \frac{\epsilon_u}{\epsilon_0} \tag{4}$$

Table 4. Results of stub column tests.

Specimen	Test	a [mm]	$N_{u.exp}$ [kN]	\bar{N}_u [-]	$\delta_{u.exp}$ [mm]	$\bar{\delta}_u(\bar{\epsilon}_u)$ [-]
SHS40	a	120.05	58.30	1.05	0.87	2.96
	b	120.12	57.53	1.04	0.86	2.92
	c	130.43	55.55	1.01	0.51	1.60
SHS60	a	181.10	92.26	0.85	0.59	0.96
	b	180.80	85.62	0.79	0.61	0.99
SHS80	a	240.12	79.50	0.58	0.60	0.76
	b	240.32	87.18	0.63	0.64	0.81
SHS100	a	300.10	90.22	0.62	0.62	0.58
	b	299.00	80.85	0.55	0.61	0.75

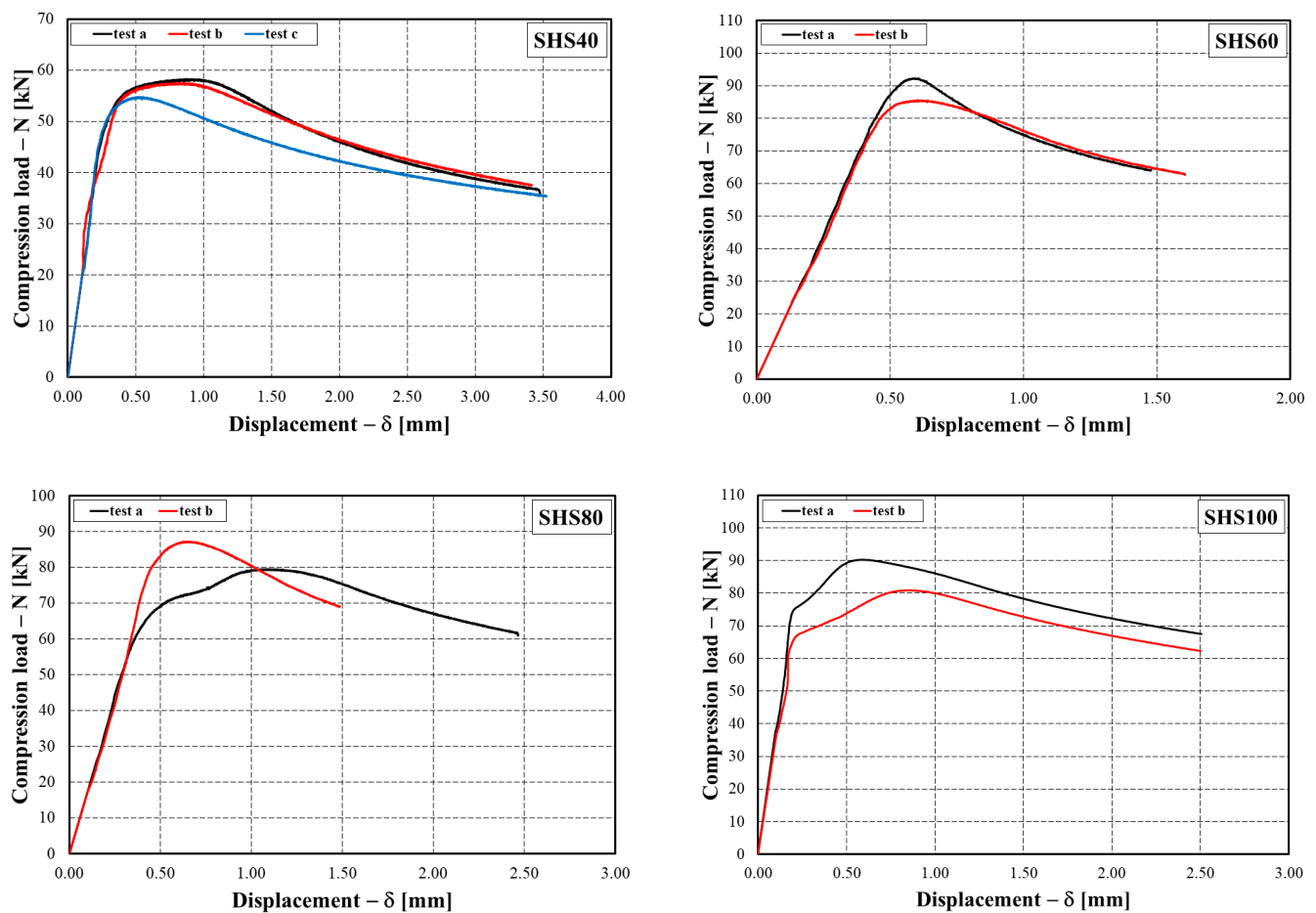


Figure 4. Experimental curve relating compression load N to displacement δ .

3. New Theoretical Procedures

3.1. Theoretical Approach Based on J2 Theory

Recently, a new theoretical approach has been developed to evaluate the ultimate compression load of aluminium members under uniform compression by considering the local buckling effects in the elastic-plastic region. This procedure is based on the J2 deformation theory of plasticity. Starting from the J2 theory [18], the plate stability equation is derived in the elastic-plastic range by including the variability of the Poisson’s ratio depending on the stress level as follows [20]:

$$C_1 \frac{\partial^4 w}{\partial x^4} + 2C_3 \frac{\partial^4 w}{\partial x^2 \partial y^2} + C_5 \frac{\partial^4 w}{\partial y^4} = - \frac{N}{D_s} \frac{\partial^2 w}{\partial x^2} \tag{5}$$

where D_s represents the secant flexural stiffness of the plate:

$$D_s = \frac{E_s t^3}{12(1 - \nu^2)} \tag{6}$$

and the coefficients C_i accounts for the nonlinear behaviour of the material:

$$\begin{aligned} C_1 &= 1 - \frac{(2-\nu)^2}{4H(1-\nu^2)} \left(1 - \frac{E_t}{E_s}\right) & C_5 &= 1 - \frac{(1-2\nu)^2}{4H(1-\nu^2)} \left(1 - \frac{E_t}{E_s}\right) \\ C_3 &= 1 + \frac{(2-\nu)(1-2\nu)}{4H(1-\nu^2)} \left(1 - \frac{E_t}{E_s}\right) & H &= 1 + \frac{(1-2\nu)^2}{4(1-\nu^2)} \left(1 - \frac{E_t}{E_s}\right) \end{aligned} \tag{7}$$

where E_s and E_t indicates the secant and tangent modulus, respectively, and ν is the Poisson’s ratio, and according to Gerard and Wildhorn [22], it can be expressed as:

$$\nu = \nu_p - (\nu_p - \nu_e) \frac{E_s}{E} = \frac{1}{2} - \left(\frac{1}{2} - \nu_e \right) \frac{E_s}{E} \tag{8}$$

The solution of Equation (5) can be defined in the Levy’s form, as reported in [18]. The final solution is expressed as:

$$w(x, y) = (A_1 \cosh \alpha y + A_2 \sinh \alpha y + A_3 \cos \beta y + A_4 \sin \beta y) \sin kx \tag{9}$$

where:

$$\alpha = \sqrt{\frac{C_3 k^2}{C_5} + \sqrt{\left(\frac{C_3}{C_5}\right)^2 k^4 - k^2 \left(k^2 \frac{C_1}{C_5} - \frac{N}{D_s C_5}\right)}} \quad \beta = \sqrt{-\frac{C_3 k^2}{C_5} + \sqrt{\left(\frac{C_3}{C_5}\right)^2 k^4 - k^2 \left(k^2 \frac{C_1}{C_5} - \frac{N}{D_s C_5}\right)}} \tag{10}$$

In order to investigate the interactive local buckling of box-shaped sections, the Equation (9) can be applied to the plate elements constituting the member sections. In particular, according to Figure 5, eight integration constants have to be derived to get:

$$\begin{aligned} \text{Plate 1 : } & \left(A_1^{(1)} \cosh \alpha_1 y_1 + A_2^{(1)} \sinh \alpha_1 y_1 + A_3^{(1)} \cos \beta_1 y_1 + A_4^{(1)} \sin \beta_1 y_1 \right) \sin kx \\ \text{Plate 2 : } & \left(A_1^{(2)} \cosh \alpha_2 y_2 + A_2^{(2)} \sinh \alpha_2 y_2 + A_3^{(2)} \cos \beta_2 y_2 + A_4^{(2)} \sin \beta_2 y_2 \right) \sin kx \end{aligned} \tag{11}$$

The following boundary conditions can be applied:

$$\begin{aligned} (1) \quad \frac{\partial w_1}{\partial y_1} \Big|_{y_1=0} &= 0 & (2) \quad R_{x.1}^* \Big|_{y_1=0} &= 0 \\ (3) \quad \frac{\partial w_2}{\partial y_2} \Big|_{y_2=0} &= 0 & (4) \quad R_{x.2}^* \Big|_{y_2=0} &= 0 \\ (5) \quad w_1 \Big|_{y_1=b_1} &= 0 & (6) \quad w_2 \Big|_{y_2=-b_2} & \\ (7) \quad \frac{\partial w_1}{\partial y_1} \Big|_{y_1=b_1} &= \frac{\partial w_2}{\partial y_2} \Big|_{y_2=-b_2} & (8) \quad M_y \Big|_{y_1=b_1} &= M_y \Big|_{y_2=-b_2} \end{aligned} \tag{12}$$

where $R_{x.i}^*$ are the equivalent shear actions while M_y represents the bending moments. By substituting Equation (9) into the relations provided in Equation (12), a system of four equations is obtained and it can be expressed in matrix form:

$$\begin{bmatrix} \cosh \alpha_1 b_1 & \cos \beta_1 b_1 & 0 & 0 \\ 0 & 0 & \cosh \alpha_2 b_2 & \cos \beta_2 b_2 \\ \alpha_1 \sinh \alpha_1 b_1 & -\beta_1 \sin \beta_1 b_1 & \alpha_2 \sinh \alpha_2 b_2 & -\beta_2 \sin \beta_2 b_2 \\ D_s^{(1)} \alpha_1^2 \cosh \alpha_1 b_1 & -D_s^{(1)} \beta_1^2 \cos \beta_1 b_1 & -D_s^{(2)} \alpha_2^2 \cosh \alpha_2 b_2 & D_s^{(2)} \beta_2^2 \cos \beta_2 b_2 \end{bmatrix} \begin{Bmatrix} A_1^{(1)} \\ A_3^{(1)} \\ A_1^{(2)} \\ A_3^{(2)} \end{Bmatrix} = \begin{Bmatrix} 0 \\ 0 \\ 0 \\ 0 \end{Bmatrix} \tag{13}$$

A trivial solution $\underline{A} = 0$ can be neglected. A non-trivial result is obtained by imposing the determinant of the coefficient matrix is equal to zero. The buckling stress corresponding to the solution of Equation (13) can be determined by means of a numerical procedure that works to increase the axial stress values in the plate elements until satisfying Equation (13).

3.2. Extension of Effective Thickness Method (ETM)

In prEN1999-1-1 Annex L [17], an extension of the effective thickness method (ETM) that incorporates buckling in the elastic-plastic range is introduced.

This approach is aimed at enhancing the accuracy in assessing the nonlinear response of aluminium structural elements subjected to uniform compression and non-uniform bending. It represents a more advanced version of the conventional effective thickness

method typically used for considering the effects of elastic local buckling in class 4 sections. The refined ETM relies on a strain-dependent analysis of the effective thickness that accounts for local buckling in the elastic-plastic region and the interaction between the plate components forming the section of the member.

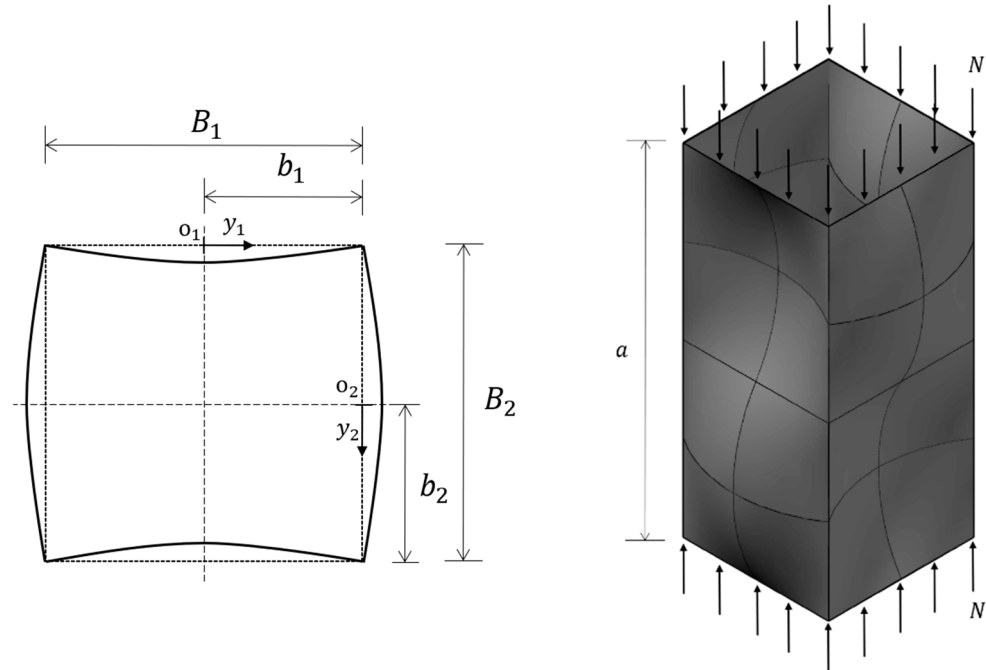


Figure 5. Geometric scheme of box members under uniform compression.

The slenderness parameter of the plate elements constituting the section is evaluated as a function of the strain level ϵ [18] as:

$$\frac{\beta}{\epsilon_0} = 17.54\eta \frac{b}{t} \sqrt{\frac{\epsilon}{\mu\zeta}} \tag{14}$$

In accordance with Eurocode 9, β denotes the slenderness parameter, which is a function of the ratio between the width b and thickness t of the plate. ϵ_0 is a non-dimensional parameter determined by the yield strength of the aluminium material and it is equal to $\sqrt{250/f_{0.2}}$. On the other hand, k represents the buckling factor, which considers the edge-restraining conditions and the stress distribution along the loaded edges. The factors η and μ are computed as:

$$\eta = \frac{2}{\sqrt{k}} \quad \mu = \frac{\zeta E}{E_s} \frac{1}{1 - \nu^2} \tag{15}$$

ζ is a correction factor accounting for interactive buckling and it is equal to $\zeta = k/k_0$ where the buckling factor k accounts for interactive buckling and k_0 is a buckling factor for an isolated plate element. In the case of plate elements, acting as a flange, connected to webs on both edges:

$$\zeta = 1.75 - \frac{0.45b_2/b_1}{0.15 + b_2/b_1} - 0.02275(b_2/b_1)^3 \geq 1 \tag{16}$$

here according to, $b_2 = B_2 - t_f$ and $b_1 = B_1 - t_w$. Equation (16) is derived from the expression of k given by BS5950-5 [23] considering that, in this case, $k_0 = 4$.

The coefficient ζ accounts for the nonlinear behaviour of the material, i.e., local buckling in the elastic-plastic range, according to the following relation:

$$\zeta = \frac{E_s}{E} \left[\frac{n-8}{8} + \frac{8}{n} \sqrt{\frac{E_t}{E_s}} \right] \tag{17}$$

The application of the effective thickness method requires a procedure under displacement control. For increasing values of the axial displacement δ , the corresponding average strain $\varepsilon = \delta/a$ is determined. Therefore, the slenderness parameter is given by Equation (14) and it increases for increasing values of ε . Then, the effective thickness can be obtained for all the plate elements and the effective cross-section area A_{eff} can be computed. The axial force corresponding to δ is computed as $N = \sigma A_{eff}$ where σ is the stress level corresponding to ε , evaluated according to the Ramberg–Osgood model. So, the axial force-displacement curve can be provided. The maximum value of this curve is the ultimate buckling load.

4. Comparison with Available Experimental Results

A comparison between the experimental results with those derived by European provisions and theoretical procedures has been provided. In particular, according to EN1999-1-1 [4], the following relation is used to predict the maximum compression resistance:

$$N_{u,EC9} = \frac{f_{0.2} A_{eff}}{\gamma_{M1}} \quad (18)$$

Obviously, in the sections belonging to first, second, or third class, A_{eff} coincides with the whole cross-section area, while in the case of the fourth class, A_{eff} is reduced due to local buckling effects. The safety factor γ_{M1} is assumed equal to 1.00.

In addition to the experimental data provided in Section 2, the comparison has been performed by considering the experimental results provided by Faella et al. [6] and Su et al. [7]. A summary of the comparison between the experimental values with theoretic values obtained by EN1999-1-1 and the theoretical procedures is reported in Table 5.

Table 5. Comparison between experimental and theoretical values.

Section	Design Code EN 1999-1-1	Deformation Theoretical Procedure (DTP)		Effective Thickness Method (ETM)	
		$\frac{N_{u,DTP}}{N_{u,exp}}$	$\frac{\bar{\varepsilon}_{u,DTP}}{\bar{\varepsilon}_{u,exp}}$	$\frac{N_{u,ETM}}{N_{u,exp}}$	$\frac{\bar{\varepsilon}_{u,ETM}}{\bar{\varepsilon}_{u,exp}}$
SHS, RHS	$\frac{N_{u,EC9}}{N_{u,exp}}$	$\frac{N_{u,DTP}}{N_{u,exp}}$	$\frac{\bar{\varepsilon}_{u,DTP}}{\bar{\varepsilon}_{u,exp}}$	$\frac{N_{u,ETM}}{N_{u,exp}}$	$\frac{\bar{\varepsilon}_{u,ETM}}{\bar{\varepsilon}_{u,exp}}$
Mean [μ]	0.93	1.02	0.99	0.96	0.81
Standard deviation [σ]	0.09	0.09	0.18	0.07	0.22

It is immediately observed that in the prediction of the maximum resistance the accuracy is very high. In fact, the mean value of the $N_{u,DTP}/N_{u,exp}$ ratios is equal to 1.02. Moreover, an important advantage of the new methodologies is related to the possibility to estimate the non-dimensional strains corresponding to the maximum compression load. Also, regarding the prediction of non-dimensional strains $\bar{\varepsilon}_u$, the values provided by the DTP procedure are very close to the experimental values. In fact, the mean value of the $\bar{\varepsilon}_{u,DTP}/\bar{\varepsilon}_{u,exp}$ ratios is equal to 0.99 with a standard deviation of 0.18. However, the great advantage of the ETM procedure is that it allows for the determination of a continuous curve between the axial load and the non-dimensional strain by also including the softening branch due to the post-buckling behaviour. This phenomenon occurs when the gradual decrease in the effective thickness is no longer counterbalanced by the corresponding increase in stress caused by the rise in strain magnitude.

For comprehensive references, all numerical values can be found in Appendix A.

5. Conclusions

In this study, the local buckling phenomenon of aluminium members subjected to uniform compression was analyzed within the elastic-plastic region. Specifically, new experimental tests were conducted on square hollow sections (SHS) made of 6060 aluminium alloys. Subsequently, novel theoretical approaches were presented. The first one is

based on the application of the J2 deformation theory of plasticity. The second method is an extension of the effective thickness method (ETM) outlined in Annex L of prEN1999-1-1. To assess the accuracy of these new methodologies, a comparison was made between the experimental results of the stub column tests and the values obtained using the European provisions and the new methods. The results revealed that the European rules underestimate the actual behavior of aluminium members subjected to uniform compression. On the other hand, the new methods demonstrate a high level of accuracy. Specifically, both the fully theoretical approach and the effective thickness method were investigated by comparing the predicted buckling resistance with the results from available experimental tests. The obtained outcomes demonstrated that the average ratio of $N_{u.th} / N_{u.exp}$ between the theoretical and experimental values of the buckling resistance is 1.02, with a standard deviation of 0.09. When applying the effective thickness method, the same ratio has an average value of 0.96 with a standard deviation of 0.07. Consequently, despite its simplicity, the effective thickness method provides satisfactory results for code provisions. Finally, these methodologies also offer the advantage of estimating the non-dimensional strains corresponding to the maximum compression loads.

Author Contributions: Conceptualization, V.P.; methodology, V.P., software, A.P.; validation, A.P.; formal analysis, A.P.; investigation, A.P.; writing—original draft, A.P.; writing—review & editing, V.P.; supervision, V.P. All authors have read and agreed to the published version of the manuscript.

Funding: This research received no external funding.

Institutional Review Board Statement: Not applicable.

Informed Consent Statement: Not applicable.

Data Availability Statement: All data are reported in Appendix A.

Conflicts of Interest: The authors declare no conflict of interest.

Appendix A

Table A1. Comparison between the theoretical ultimate loads with the experimental results provided by Faella et al. [6].

Specimen	$N_{u.exp}$ [kN]	$N_{u.EC9}$ [kN]	$N_{u.DTP}$ [kN]	$N_{u.ETM}$ [kN]	Specimen	$N_{u.exp}$ [kN]	$N_{u.EC9}$ [kN]	$N_{u.DTP}$ [kN]	$N_{u.ETM}$ [kN]		
SHS1	A	30.6	21.44	25.47	25.05	RHS8	B	212	198.11	209.29	197.37
	B	29.7	21.44	25.47	25.05	RHS9	A	222.6	227.86	232.03	212.50
SHS2	A	158.4	131.57	155.94	152.98		B	224.9	227.86	232.03	212.50
	B	160.8	131.57	155.95	152.98	RHS10	A	271.2	279.03	296.30	250.31
SHS3	A	132.4	130.43	139.00	136.29		B	255.6	279.03	296.30	250.31
	B	131.3	130.43	139.00	136.29	RHS11	A	290.8	275.92	312.79	236.38
SHS4	A	186.6	159.29	174.22	171.79		B	261.2	250.83	312.79	236.38
	B	180.9	159.29	174.22	171.79	RHS12	A	313.2	250.83	336.21	260.00
SHS5	A	213.8	191.34	208.81	203.64		B	315.6	284.01	335.99	265.00
	B	208.7	191.34	208.81	203.64	RHS13	A	248.1	243.08	248.44	248.00
SHS6	A	264.4	251.49	265.75	259.65		B	248.2	243.08	248.44	228.33
	B	263.8	251.49	265.75	259.65	RHS14	A	85.1	85.90	89.02	80.50
SHS7	A	300.2	316.13	320.23	305.19		B	79.1	85.90	89.02	80.50
	B	304.8	316.13	320.25	305.19		C	79.7	85.90	89.02	80.50

Table A1. *Cont.*

Specimen	$N_{u,exp}$ [kN]	$N_{u,EC9}$ [kN]	$N_{u,DTP}$ [kN]	$N_{u,ETM}$ [kN]	Specimen	$N_{u,exp}$ [kN]	$N_{u,EC9}$ [kN]	$N_{u,DTP}$ [kN]	$N_{u,ETM}$ [kN]		
SHS8	A	82.7	83.20	86.49	80.53	RHS15	A	185.7	166.53	176.42	168.19
	B	83.3	83.20	86.49	80.53		B	190.7	166.53	176.42	168.19
SHS9	A	84.7	81.03	107.85	92.33	RHS16	C	185.2	166.53	176.41	168.19
	B	84.6	81.03	107.85	92.33		A	92.5	90.14	99.49	83.03
SHS10	A	728.5	664.13	706.27	686.75	RHS17	B	92.8	90.14	99.49	83.03
	B	731.5	664.13	706.27	686.75		A	89.4	81.80	87.67	78.14
SHS11	A	605.5	540.06	577.65	509.27	RHS18	B	88.6	81.80	87.67	78.14
	B	592.5	540.06	577.55	509.27		A	92.7	94.92	116.27	92.35
SHS12	A	626.5	605.82	721.78	626.40	RHS19	B	89.4	87.00	115.72	92.35
	B	643.5	605.82	721.77	626.40		A	137.7	132.00	166.64	143.78
RHS1	A	78.7	62.99	71.77	70.00	RHS20	B	139.6	132.00	166.78	143.78
	B	77.5	62.99	71.77	70.00		A	513.5	529.34	535.33	474.27
RHS2	A	124.3	99.87	111.39	109.26	RHS21	B	506.5	529.34	535.33	474.27
	B	122.4	99.87	111.36	109.26		A	115.3	117.40	124.58	121.58
RHS3	A	134.8	106.32	118.72	116.00	RHS22	B	116.5	117.40	124.58	121.58
	B	136.8	106.32	118.72	115.50		A	493	525.32	571.11	496.62
RHS4	A	109.8	98.12	109.19	104.19	RHS23	B	497	525.32	571.11	496.62
	B	109.2	98.12	109.22	104.19		A	621.5	631.77	708.55	611.11
RHS5	A	108.5	101.89	105.45	103.46	RHS24	B	612	631.77	708.55	611.11
	B	109.1	101.24	104.78	103.46		A	2939.4	2743.00	3016.10	2929.40
RHS6	A	122.4	112.58	122.53	115.24	RHS25	B	2934	2743.00	3016.12	2929.40
	B	122.9	112.58	122.47	115.24		A	669	664.00	748.64	714.22
RHS7	A	120.6	113.90	116.88	108.88	RHS26	B	670.5	672.07	748.64	714.22
	B	118.7	113.90	116.87	108.88		A	865	771.97	802.70	780.13
RHS8	A	212	198.11	209.30	197.37	B	852	771.97	802.70	780.13	

Table A2. Comparison between the theoretical values with the experimental results provided in Section 2 and by Su et al. [7].

Specimen	$N_{u,exp}$ [kN]	$N_{u,EC9}$ [kN]	$N_{u,DTP}$ [kN]	$N_{u,ETM}$ [kN]	Specimen	$N_{u,exp}$ [kN]	$N_{u,EC9}$ [kN]	$N_{u,DTP}$ [kN]	$N_{u,ETM}$ [kN]		
SHS40	A	58.3	50.38	56.82	56.21	H64 × 64 × 3	A	164.2	160.68	170.16	148.13
	B	57.53	50.38	56.82	56.09		B	165.4	162.86	173.28	150.54
	C	55.55	50.38	55.00	56.09	H70 × 55 × 4.2	A	196.2	183.69	200.46	191.31
SHS60	A	92.26	89.62	94.38	87.65	H95 × 50 × 10.5	B	196.9	184.11	200.98	191.74
	B	85.62	89.62	94.38	87.65		A	626.2	587.32	613.59	722.86
SHS80	A	79.5	88.11	85.12	81.21	H120 × 70 × 10.5	A	862.5	793.77	840.28	924.23
	B	87.18	88.11	85.12	81.21	H120 × 120 × 9	A	981.5	890.83	882.53	987.83
SHS100	A	90.22	78.70	96.12	89.86	N95 × 50 × 10.5	A	609.8	459.83	572.61	574.76
	B	80.85	78.70	96.12	89.86	N120 × 70 × 10.5	A	736.9	490.38	684.69	583.69
					N120 × 120 × 9	A	811.1	717.36	769.20	812.48	

Table A3. Comparison between the non-dimensional strains with the experimental results provided by Faella et al. [6].

Specimen		$\bar{\epsilon}_{u.exp}$ [-]	$\bar{\epsilon}_{u.DTP}$ [-]	$\bar{\epsilon}_{u.ETM}$ [-]	Specimen		$\bar{\epsilon}_{u.exp}$ [-]	$\bar{\epsilon}_{u.DTP}$ [-]	$\bar{\epsilon}_{u.ETM}$ [-]
SHS1	A	30.04	31.00	21.73	RHS8	B	2.88	3.52	3.10
	B	32.51	30.95	21.73	RHS9	A	1.95	2.49	0.98
SHS2	A	18.36	17.80	12.69		B	1.88	2.49	0.98
	B	21.07	17.81	12.69	RHS10	A	1.60	1.82	1.06
SHS3	A	4.94	4.73	3.12		B	1.35	1.20	1.06
	B	5.07	4.73	3.12	RHS11	A	1.09	1.16	1.14
SHS4	A	11.65	10.92	7.46		B	1.09	1.16	1.14
	B	13.26	10.92	7.46	RHS12	A	1.04	0.96	0.99
SHS5	A	6.88	5.93	3.95		B	0.99	0.96	0.99
	B	7.89	5.93	3.95	RHS13	A	1.95	2.33	1.06
SHS6	A	3.52	4.30	2.77		B	1.88	2.00	1.06
	B	4.13	4.30	2.77	RHS14	A	1.24	1.27	1.05
SHS7	A	1.43	1.99	1.23		B	1.26	1.20	1.05
	B	1.47	1.99	1.23	RHS15	A	4.64	4.50	3.21
SHS8	A	1.90	2.49	1.60		B	4.16	4.50	3.21
	B	1.71	2.49	1.60	RHS16	C	5.21	4.50	3.21
SHS9	A	0.81	0.70	0.91		A	1.12	0.92	0.95
	B	0.76	0.70	0.91	B	1.08	0.92	0.95	
SHS10	A	2.91	3.39	2.13	RHS17	A	1.24	1.39	1.03
	B	3.26	3.39	2.13		B	1.28	1.39	1.03
SHS11	A	1.56	1.47	1.17	RHS18	A	0.98	0.79	0.95
	B	1.29	1.47	1.17		B	1.02	0.78	0.95
SHS12	A	1.13	1.19	1.07	RHS19	A	0.83	0.85	0.99
	B	1.06	1.19	1.07		B	0.83	0.85	0.99
RHS1	A	19.41	13.64	11.98	RHS20	A	0.89	0.83	0.80
	B	19.39	13.64	11.98		B	0.93	0.83	0.80
RHS2	A	24.93	21.69	18.76	RHS21	A	2.77	2.00	2.79
	B	24.54	21.56	18.76		B	3.26	3.00	2.79
RHS3	A	15.10	13.21	10.11	RHS22	A	0.97	0.81	0.95
	B	15.12	13.21	10.14		B	0.92	0.81	0.95
RHS4	A	6.70	6.36	4.20	RHS23	A	1.00	1.00	0.96
	B	6.45	6.39	4.20		B	0.99	0.98	0.96
RHS5	A	3.75	4.34	2.33	RHS24	A	2.83	2.83	1.01
	B	3.28	4.36	2.33		B	2.85	2.70	1.01
RHS6	A	3.83	4.62	3.05	RHS25	A	1.37	1.37	1.26
	B	4.15	4.59	3.05		B	1.39	1.37	1.26
RHS7	A	1.94	1.50	1.13	RHS26	A	1.95	1.39	1.13
	B	1.63	1.50	1.13		B	1.92	1.39	1.13
RHS8	A	2.90	3.52	3.10					

Table A4. Comparison between the non-dimensional strains with the experimental results provided in Section 2 and by Su et al. [7].

Specimen	$\bar{\epsilon}_{u,exp}$ [-]	$\bar{\epsilon}_{u,DTP}$ [-]	$\bar{\epsilon}_{u,ETM}$ [-]	Specimen	$\bar{\epsilon}_{u,exp}$ [-]	$\bar{\epsilon}_{u,DTP}$ [-]	$\bar{\epsilon}_{u,ETM}$ [-]		
SHS40	A	2.94	2.96	2.05	H64 × 64 × 3	A	2.14	2.18	1.14
	B	2.90	2.92	2.05		B	2.20	2.25	1.15
	C	1.60	1.60	2.05		A	5.67	5.69	2.69
SHS60	A	0.97	0.96	0.93	H70 × 55 × 4.2	B	5.70	5.72	2.69
	B	0.99	0.99	0.93	H95 × 50 × 10.5	A	2.07	2.05	2.43
SHS80	A	1.38	0.76	0.84	H120 × 70 × 10.5	A	2.17	2.14	2.60
	B	0.80	0.81	0.84	H120 × 120 × 9	A	1.61	1.50	2.00
SHS100	A	1.08	0.58	0.83	N95 × 50 × 10.5	A	8.24	8.16	8.51
	B	1.41	0.75	0.83	N120 × 70 × 10.5	A	22.11	22.00	21.70
					N120 × 120 × 9	A	2.56	2.50	3.47

References

- Mazzolani, F.M. 3D aluminium structures. *Thin Walled Struct.* **2012**, *61*, 258–266. [\[CrossRef\]](#)
- Georgantzia, E.; Gkantou, M.; Kamaris, G.S. Aluminium alloys as structural material: A review of research. *Eng. Struct.* **2021**, *227*, 111372. [\[CrossRef\]](#)
- Pisapia, A.; Natri, E.; Piluso, V.; Formisano, A.; Mazzolani, F.M. Experimental campaign on structural aluminium alloys under monotonic and cyclic loading. *Eng. Struct.* **2023**, *282*, 115836. [\[CrossRef\]](#)
- EN 1999-1; Eurocode 9: Design of Aluminium Structures—Part 1.1: General Structural Rules. European Committee for Standardization: Brussels, Belgium, 2007.
- EN 1993-1; Eurocode 3: Design of Steel Structures—Part 1.1: General Rules and Rules for Buildings. European Committee for Standardization: Brussels, Belgium, 2005.
- Faella, C.; Mazzolani, F.M.; Piluso, V.; Rizzano, G. Local buckling of aluminium members: Testing and classification. *J. Struct. Eng.* **2000**, *126*, 353–360. [\[CrossRef\]](#)
- Su, M.N.; Young, B.; Gardner, L. Testing and design of aluminium alloy cross sections in compression. *J. Struct. Eng.* **2014**, *140*, 04014047. [\[CrossRef\]](#)
- Moen, L.A.; Hopperstad, O.S.; Langseth, M. Rotational capacity of aluminium beams under moment gradient. I: Experiments. *J. Struct. Eng.* **1999**, *125*, 910–920. [\[CrossRef\]](#)
- Wang, Y.Q.; Wang, Z.X.; Yin, F.X.; Yang, L.; Shi, Y.J.; Yin, J. Experimental study and finite element analysis on the local buckling behavior of aluminium alloy beams under concentrated loads. *Thin-Walled Struct.* **2016**, *105*, 44–56. [\[CrossRef\]](#)
- Piluso, V.; Pisapia, A.; Natri, E.; Montuori, R. Ultimate resistance and rotation capacity of low yielding high hardening aluminium alloy beams under non-uniform bending. *Thin-Walled Struct.* **2019**, *135*, 123–136. [\[CrossRef\]](#)
- Montuori, R.; Natri, E.; Piluso, V.; Pisapia, A. Ultimate behaviour of high-yielding low-hardening aluminium alloy I-beams. *Thin-Walled Struct.* **2020**, *146*, 106463. [\[CrossRef\]](#)
- Montuori, R.; Natri, E.; Piluso, V.; Pisapia, A. The influence of the material properties on the ultimate behaviour of aluminium H-shaped beams. *Open Constr. Build.* **2021**, *15*, 176–188. [\[CrossRef\]](#)
- Pisapia, A. FEM calibration for aluminium I-beams under moment gradient. In Proceedings of the International Conference on Numerical Analysis and Applied Mathematics, Rhodes, Greece, 13 September 2018.
- Pisapia, A. Empirical formulas to predict the ultimate behaviour of I-shaped aluminium members. In Proceedings of the International Conference on Numerical Analysis and Applied Mathematics, Rhodes, Greece, 23 September 2020.
- Natri, E.; Piluso, V.; Pisapia, A. Numerical application of effective thickness approach to box aluminium sections. *J. Comps. Sci* **2021**, *5*, 291. [\[CrossRef\]](#)
- Natri, E.; Piluso, V.; Pisapia, A. Experimental tests on SHS aluminium beams under non-uniform bending. *Eng. Struct.* **2022**, *267*, 114649. [\[CrossRef\]](#)
- CEN/TC250/SC9 N888-prEN 1999-1; Eurocode 9: Design of Aluminium Structures—Part 1.1: General Structural Rules. European Committee for Standardization: Brussels, Belgium, 2018.
- Piluso, V.; Pisapia, A. Interactive plastic local buckling of box-shaped aluminium members under uniform compression. *Thin Walled Struct.* **2021**, *164*, 107828. [\[CrossRef\]](#)
- Piluso, V.; Pisapia, A.; Rizzano, G. Local buckling of aluminium channels under uniform compression: Theoretical analysis and experimental tests. *Thin Walled Struct.* **2022**, *179*, 109511. [\[CrossRef\]](#)
- Piluso, V.; Pisapia, A. Theoretical procedure to predict the local buckling resistance of aluminium members in elastic-plastic range. In Proceedings of the World Congress in Computational Mechanics and ECCOMAS Congress, Oslo, Norway, 5 June 2022.

21. *UNI EN ISO 6892-1*; Metallic Materials—Tensile Testing—Part 1: Method of Test at Room Temperature. European Standard, European Committee for Standardization: Brussels, Belgium, 2020.
22. Gerard, G.; Wildhorn, S. *A Study of Poisson's Ratio in the Yield Region*; National Advisory Committee for Aeronautics (NACA) Technical Note 2561; National Advisory Committee for Aeronautics (NACA): Washington, DC, USA, 1952.
23. *BS 5950-5*; Structural Use of Steelwork in Building—Formed Thin Gauge. Part 5: Code Practice for Design of Cold Formed Thin Gauge Sections. Steel Construction Institute: Ascot, UK, 1998.

Disclaimer/Publisher's Note: The statements, opinions and data contained in all publications are solely those of the individual author(s) and contributor(s) and not of MDPI and/or the editor(s). MDPI and/or the editor(s) disclaim responsibility for any injury to people or property resulting from any ideas, methods, instructions or products referred to in the content.